Two-color interference stabilization of atoms

M. V. Fedorov* and N. P. Poluektov[†]

General Physics Institute, Russian Academy of Science, 38, Vavilov Street, Moscow 117942, Russia

The effect of interference stabilization is shown to exist in a system of two atomic levels coupled by a strong two-color laser field, the two frequencies of which are close to a two-photon Raman-type resonance between the chosen levels, with open channels of one-photon ionization from both of them. We suggest an experiment, in which a rather significant (up to 90%) suppression of ionization can take place and which demonstrates explicitly the interference origin of stabilization. Specific calculations are made for H and He atoms and optimal parameters of a two-color field are found. The physics of the effect and its relation with such well-known phenomena as light induced continuum structure and population trapping in a three-level system are discussed.

I. INTRODUCTION

A. Interference stabilization

Interference stabilization of Rydberg atoms, or strong-field suppression of photoionization, is known [1,2] to be a phenomenon related to the coherent repopulation of levels neighboring the initially populated one. Such a repopulation arises owing to Raman-type transitions via the continuum and in the case of a single-color field it can be efficient only if the field is strong enough. Specifically, the strong-field criterion for the effect of interference stabilization is formulated qualitatively as the requirement for the ionization width $\Gamma_i^{(n)}$ of the initially populated atomic level E_n to be larger than the spacing between neighboring levels

$$\Gamma_i^{(n)} > |E_n - E_{n\pm1}|, \tag{1}$$

where n is the principal quantum number. The ionization width is determined here as the rate of ionization calculated with the help of the Fermi golden rule. However, repopulation of neighboring Rydberg levels is provided, actually, by the off-diagonal terms of the tensor of ionization widths $\Gamma_i^{(n',n)}$. In the approximation of adiabatic elimination of the continuum (which includes, in particular, the well-known rotating wave approximation [2]) this tensor is determined as a direct generalization of the Fermi golden rule expression for $\Gamma_i^{(n)}$

$$\Gamma_i^{(n',n)} = \left. \frac{\pi}{2}\varepsilon_0^2 \langle n'|d|E\rangle\langle E|d|n\rangle \right|_{E=E_n+\omega}, \tag{2}$$

where ε_0 and ω are the laser field-strength amplitude and frequency, d is the projection of the atomic dipole moment upon the direction of light polarization, E is the energy of the atomic electron in the continuum, and atomic units are used throughout the paper if not indicated differently. So, the next crucial assumption in the theory of interference stabilization

is that all the components of the tensor (2) are approximately equal to each other

$$\Gamma_i^{(n',n)} \approx \Gamma. \tag{3}$$

This assumption is pretty well fulfilled for high atomic Rydberg levels $n,n' \gg 1, |n-n'| \ll n$ (see explanations in Ref. [2]). It should be noted also that for Rydberg levels their ac Stark shift, as well as the shift of the ionization threshold are equal approximately to the ponderomotive energy $\varepsilon_0^2/4\omega^2$ and identical to each other, and this common shift does not affect either the dynamics of photoionization from Rydberg levels or the effect of interference stabilization.

The simplest model, in which the effect of interference stabilization exists, is the model of two close atomic levels E_1 and E_2 connected with each other by the Raman-type transitions via the continuum, for which the conditions (1) and (3) are fulfilled and the ac Stark shift has the same features as described above for Rydberg levels and, actually, can be ignored. In both two-level and multilevel systems there are several different theoretical approaches one can use to solve the problems of strong-field photoionization and stabilization. One of them is based on the use of quasienergy or "dressed-state" analysis. The total wave function of an atomic electron in a light field can be expanded in a series of the field-free atomic eigenfunctions

$$\Psi = \sum_n C_n(t)\psi_n + (\text{continuum}). \tag{4}$$

In the approximation of adiabatic elimination of the continuum equations for the coefficients $C_n(t)$ are stationary, and in the simplest case of the two-level system they have the form

$$i\dot{C}_1(t) - E_1 C_1(t) = -\frac{i}{2}\Gamma\left[C_1(t) + C_2(t)\right],$$

$$i\dot{C}_2(t) - E_2 C_2(t) = -\frac{i}{2}\Gamma\left[C_1(t) + C_2(t)\right], \tag{5}$$

where the approximation (3) is assumed to be fulfilled.

---

*Electronic address: fedorov@ran.gpi.ru
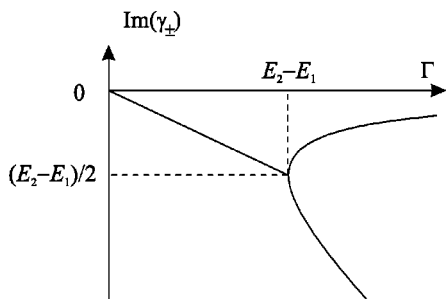
[†]Electronic address: nickel@aha.ru

FIG. 1. The functions $\mathrm{Im}[\gamma_\pm(\Gamma)]$ (6).

As Eqs. (5) are stationary, they have solutions of the form $C_{1,2} \propto \exp(-i\gamma t)$, where γ is a complex quasienergy. When this exponential dependence on t is substituted into Eqs. (5), they turn into a set of two algebraic homogeneous equations, which has a nonzero solution if its determinant turns zero. This is the condition from which the two quasienergies of the field-driven two-level system have to be found, and the result is given by

$$\gamma_\pm = \frac{1}{2}\{E_1 + E_2 - i\,\Gamma \pm \sqrt{(E_2 - E_1)^2 - \Gamma^2}\}. \qquad (6)$$

From here we see that, indeed, a drastic change in the form of the solutions occurs when the interaction constant Γ becomes larger than the level spacing $E_2 - E_1$. The point $\Gamma = E_2 - E_1$ is the branching point, below which (at $\Gamma < E_2 - E_1$) the root square is real in Eq. (6), whereas above the branching point (at $\Gamma > E_2 - E_1$) it becomes imaginary. The imaginary parts of the quasienergies $\gamma_\pm$ (6) are shown in Fig. 1, and they determine the field-dependent widths of the two quasienergy levels $\Gamma_\pm(\varepsilon_0) \equiv 2|\mathrm{Im}[\gamma_\pm(\Gamma)]|$, where $\Gamma \propto \varepsilon_0^2$ (2). One of the two branches arising at $\Gamma > E_2 - E_1 [\gamma_+(\Gamma)]$ corresponds to a narrowing quasienergy level whose width $\Gamma_+(\varepsilon_0)$ falls with a growing field-strength amplitude. This corresponds to an increasing lifetime of this quasienergy level and to stabilization of an atomic population at this level.

B. Laser-induced continuum structures, autoionizing resonances, dark states, and population trapping

Though rather attractive by its simplicity, an isolated two-level system obeying the requirement (3) can hardly be easily found in the usual atomic spectra. This is the reason why here we consider another scheme, in which two atomic levels with significantly different energies and bound-free dipole matrix elements are connected with each other by Raman-type transitions via the continuum in a two-color field (Fig. 2). Such a scheme has been widely discussed in the literature [3–14] in connection with the phenomenon of the light-induced continuum structure (LICS), briefly outlined below. The process we suggest and investigate, as well as its similarity and differences with LICS are discussed in Sec. I C.

In LICS, one of the two fields of a two-color light is assumed to be strong [$(\omega_2, \varepsilon_2)$, the pump] and the other one weak [$(\omega_1, \varepsilon_1)$, the probe], where $\omega_{1,2}$ and ε_{12} are the corre-
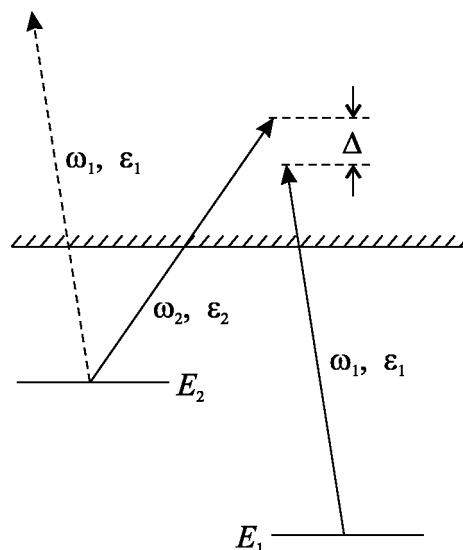

FIG. 2. A scheme of two atomic levels under the conditions of a Raman-type resonance in a two-color field.

sponding frequencies and field-strength amplitudes. In a scheme of Fig. 2, Δ is the Raman-type resonance detuning

$$\Delta = E_2 + \omega_2 - E_1 - \omega_1. \qquad (7)$$

The frequency of the pump field is assumed to be smaller then the binding energy of the initially populated level E_1, $\omega_2 < |E_1|$, to exclude a direct photoionization of an atom by this field.

Under the action of the pump the first Floquet satellite of the level E_2 takes the form of an autoionizinglike level $E_2 + \omega_2$ at the background of the continuum with the width equal to the ionization width of the level E_2, $\Gamma_i^{(2)} \equiv \Gamma_i^{(2,2)}$ (2) with ε_0 substituted by ε_2. The probe field ionizes the atom and takes the Floquet satellite $E_2 + \omega_2$ for an almost real autoionizing level, which gives rise to the typical asymmetric Fano-profile-like structure of the dispersion curve $w_i(\omega_1)$ (Fig. 3).

The Fano minimum of the curve $w_i(\omega_1)$ arises owing to interference of direct and indirect transitions to the continuum ($E_1 \rightarrow E$ and $E_1 \rightarrow E' \rightarrow E_2 \rightarrow E$). But this is not yet a stabilization understood as an increasing suppression of ionization with a growing light intensity. An experiment we suggest and discuss below can explicitly demonstrate such an interference suppression and stabilization of an atom in its
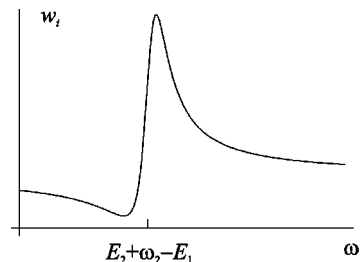

FIG. 3. The Fano profile of the dispersion curve $w_i(\omega_1)$ at an autoionizinglike resonance.

bound states. We will assume that both fields can be equally strong and in this sense the effect we consider can be referred to as a strong-field LICS.

It should be noted that the channel of ionization shown in Fig. 2 by a dashed line (taken into account for the first time in Ref. [5]) determines a nonzero height of the Fano curve in its minimum. As we will see below, this is just the competition of this noninterfering channel of ionization with interfering ones that is crucially important for optimization of stabilization in its dependence on light intensities.

At last, another well-known analogue of LICS is related to single- and double strong-field resonances at real autoionizing atomic levels [7,15–18]. The physics of this phenomenon and LICS are close though there are evident differences concerning mechanisms of level broadening. These differences make autoionizing resonances not as closely related to the phenomenon under consideration as LICS. The same can be said about dark states and population trapping in a three-level system [19–22]. The physics of all these phenomena is similar though important details are different. In particular, this concerns intensity-dependent mechanisms of level broadening and an important role of the noninterfering ionization channel specific for the scheme under consideration and missing in a three-level scheme. In addition, the atomic continuous spectrum is so much wider than any discrete third level that this makes characteristic intensities in the phenomenon to be discussed absolutely different from those in the population trapping effect.

C. An experiment we suggest

Let us assume that the initially populated level in a scheme of Fig. 2 is E_1. At the first stage, by considering ionization of an atom by the field ε_1 alone (with $\varepsilon_2=0$), we select the peak light intensity $I_1=\varepsilon_1^2/8\pi$ and pulse duration τ high and long enough to provide almost complete ionization of an atom by a pulse $w_i(I_1,I_2=0)=1$. Then, by adding the field ε_2 we expect that under proper conditions, owing to interference effect, the combined action of two fields will result in a significant suppression of ionization. In other words, we expect that the function $w_i(I_1,I_2)$ in its dependence on I_2 at a given selected value of I_1 will start from 1 at $I_2=0$, then it will have a minimum at some intensity $I_2=I_{20}$ $\sim I_1$, and then, at higher intensity I_2, $w_i(I_1,I_2)$ will return to 1 again. The region around I_{20} will be interpreted as a stabilization window. The interference origin of stabilization is evident, because with a growing I_2 (at a given I_1), we increase an energy that can be put into an atom. But, counterintuitively, this additional energy results in a slower rather than faster ionization, and this can be explained only by interference effects. We will find values of the resonance detuning Δ and the ratio of intensities I_2/I_1 which optimize the stabilization effect.

II. THE MAIN EQUATIONS

Compared to a simplified system of two close levels in a single-color field described in the Introduction, to appropriately characterize a system of Fig. 2 in a two-color arbitrary

strong field, in addition to ionization broadening and mixing of levels, we have to take into account also their shifts and mixing arising owing to the ac Stark effect. Both these effects can be described in terms of the complex polarizability tensor $\alpha_{i,j}$, $i,j=1,2$,

$$\alpha_{i,i}(\omega) \equiv \alpha_i(\omega) = \int dE|d_{i\,E}|^2\left(\frac{1}{E-E_i-\omega-i\delta} + \frac{1}{E-E_i+\omega}\right) \tag{8}$$

and

$$\alpha_{21} = \int dE d_{2E}d_{E1}\left(\frac{1}{E-E_1-\omega_1-i\delta} + \frac{1}{E-E_1+\omega_2}\right) \approx \alpha_{12}, \tag{9}$$

where integration over E includes summation over intermediate discrete states.

For the two-color scheme (Fig. 2), similarly to Eq. (4), in the rotating wave approximation the wave function of an atomic electron can be written as

$$\Psi = C_1(t)e^{i\omega_1 t}\psi_1 + C_2(t)e^{i\omega_2 t}\psi_2 + (\text{continuum}). \tag{10}$$

As well as Eqs. (5), equations for the probability amplitudes $C_1(t)$ and $C_2(t)$ are obtained from the Schrödinger equation with the help of the procedure of adiabatic elimination of the continuum. In terms of $\alpha_{i,j}$ (8),(9), these equations can be presented in the form

$$i\dot{C}_1 - [\widetilde{E}_1(t) + \omega_1]C_1 = -\frac{1}{4}\varepsilon_{10}(t)\varepsilon_{20}(t)\alpha_{12}C_2,$$

$$i\dot{C}_2 - (\widetilde{E}_2(t) + \omega_2)C_2 = -\frac{1}{4}\varepsilon_{10}(t)\varepsilon_{20}(t)\alpha_{21}\,C_1, \tag{11}$$

where $\widetilde{E}_i(t)$ are the slowly time-dependent adiabatic complex energies of the ac-Stark-shifted and broadened levels

$$\widetilde{E}_i(t) = E_i - \frac{1}{4}\{\alpha_i(\omega_1)\varepsilon_{10}^2(t) + \alpha_i(\omega_2)\varepsilon_{20}^2(t)\}. \tag{12}$$

III. QUASIENERGIES

For the time-dependent pulse envelopes $\varepsilon_{10}(t)$ and $\varepsilon_{20}(t)$, Eqs. (11) have to be solved as the initial-value problem. In the model of constant field-strength amplitudes these equations have stationary solutions $C_{1,2}\propto\exp(-i\gamma t)$, where, as previously, γ is the complex quasienergy for which we get the solutions generalizing those of Eq. (6)

$$\gamma_{\pm} = \frac{1}{2}\{\widetilde{E}_1 + \omega_1 + \widetilde{E}_2 + \omega_2 \pm D\}, \tag{13}$$

where

$$D = \sqrt{\widetilde{\Delta}^2 + \frac{1}{4}\alpha_{12}\alpha_{21}\varepsilon_{10}^2\varepsilon_{20}^2} \tag{14}$$

and $\widetilde{\Delta}$ is the time-dependent complex detuning for the ac-Stark-shifted and broadened levels (12)

$$\widetilde{\Delta} = \widetilde{E}_2 + \omega_2 - \widetilde{E}_1 - \omega_1. \tag{15}$$

Imaginary parts of the energies $\widetilde{E}_i$ (12) are related to the ionization widths determined by imaginary parts $\mathrm{Im}(\alpha_i) \equiv \alpha_i''$ of the polarizabilities α_i (8)

$$\mathrm{Im}(E_1) = -\frac{1}{2}\Gamma_1,$$

$$\mathrm{Im}(E_2) = -\frac{1}{2}(\Gamma_2^{(1)} + \Gamma_2^{(2)}), \tag{16}$$

where

$$\Gamma_1 = \frac{1}{2}\alpha_1''(\omega_1)\varepsilon_{10}^2,$$

$$\Gamma_2^{(1)} = \frac{1}{2}\alpha_2''(\omega_1)\varepsilon_{10}^2, \quad \text{and} \quad \Gamma_2^{(2)} = \frac{1}{2}\alpha_2''(\omega_2)\varepsilon_{20}^2. \tag{17}$$

The width $\Gamma_2^{(1)}$ is determined by transitions from the level E_2 under the action of the field ε_{10} (the dashed line in Fig. 2). As $E_2 > E_1$ and $\omega_1 > \omega_2$, typically,

$$\alpha_2''(\omega_1) \ll \alpha_1''(\omega_1) \quad \text{or} \quad \Gamma_2^{(1)} \ll \Gamma_1. \tag{18}$$

Similarly to Eq. (17), the off-diagonal component of the polarizability tensor (9) determines the off-diagonal component of the ionization-width tensor

$$\Gamma_{12} = \frac{1}{2}\alpha_{12}''\varepsilon_{10}\varepsilon_{20} = \sqrt{\Gamma_1 \Gamma_2^{(2)}}, \tag{19}$$

which assumes, in particular, that $\alpha_{12}'' = \sqrt{\alpha_1''(\omega_1)\alpha_2''(\omega_2)}$. Imaginary parts of quasienergies $\gamma_\pm$ (13) are related to the width of quasienergy levels $\Gamma_\pm$

$$\Gamma_\pm = -2\mathrm{Im}(\gamma_\pm). \tag{20}$$

IV. PROBABILITY OF IONIZATION

The above described quasienergy solutions of Eqs. (11) are most appropriate for solving the initial-value problem in the case of pulses with rectangular envelopes $\varepsilon_{1,20}(t)$, with sudden turn on and turn off (at $t=0$ and $t=\tau$) and $\varepsilon_{1,20}(t) = \mathrm{const}$ at $0 < t < \tau$. With known quasienergies $\gamma_\pm$ (13) the time-dependent probability amplitudes $C_{1,2}(t)$ to find an atom in its bound states ψ_1 and ψ_2 can be presented in the form

$$C_{1,2}(t) = A_{1,2}^+ \exp(-i\,\gamma_+ t) + A_{1,2}^- \exp(-i\,\gamma_- t), \tag{21}$$

where $A_{1,2}^\pm$ are constants to be found from the initial conditions

$$A_1^+ + A_1^- = 1 \quad \text{and} \quad A_2^+ + A_2^- = 0 \tag{22}$$

and from equations connecting $A_1^\pm$ with $A_2^\pm$. The latter follow, e.g., from the first of Eqs. (11)

$$\gamma_\pm A_1^\pm - (\widetilde{E}_1 + \omega_1)A_1^\pm = -\frac{1}{4}\varepsilon_{10}\varepsilon_{20}\alpha_{12} A_2^\pm. \tag{23}$$

The total residual probability $w_{\mathrm{res}}(\tau)$ to find an atom in bound states at $t=\tau$ is given by the sum of partial probabilities $w_1(\tau)$ and $w_2(\tau)$ to find an atom at levels E_1 and E_2,

$$w_{\mathrm{res}}(\tau) = w_1(\tau) + w_2(\tau), \tag{24}$$

where

$$w_{1,2}(\tau) = |C_{1,2}(\tau)|^2 = |A_{1,2}^+ e^{-i\,\gamma_+ \,\tau} + A_{1,2}^- e^{-i\,\gamma_- \tau}|^2. \tag{25}$$

The probability of ionization is given by $w_i(\tau) = 1 - w_{\mathrm{res}}(\tau)$. Equations (22) and (23) are easily solved to give, explicitly,

$$w_1(\tau) = \frac{1}{4}\left| \left(1 - \frac{\widetilde{\Delta}}{D}\right)e^{-i\gamma_+ \tau} + \left(1 + \frac{\widetilde{\Delta}}{D}\right)e^{-i\gamma_- \tau} \right|^2 \tag{26}$$

and

$$w_2(\tau) = \frac{\alpha_{12}^2 \varepsilon_{10}^2 \varepsilon_{20}^2}{16\,D^2}|e^{-i\gamma_+ \tau} - e^{-i\gamma_- \tau}|^2. \tag{27}$$

In the case of pulses with smooth envelopes $\varepsilon_{1,2}(t)$ quasienergy solutions are not so useful for solving the initial-value problem, and one has to solve directly Eqs. (11) for the time-dependent probability amplitudes $C_{1,2}(t)$.

V. SCALING EFFECT AND RELATIVE UNITS

With the help of a phase transformation

$$C_i(t) = \exp\{-i(E_1 + \omega)t\}A_i(t), \tag{28}$$

Eqs. (11) can be reduced to an asymmetric form

$$i\dot{A}_1 + \frac{1}{4}\{\alpha_1(\omega_1)\varepsilon_{10}^2(t) + \alpha_1(\omega_2)\varepsilon_{20}^2(t)\}A_1$$

$$= -\frac{1}{4}\varepsilon_{10}(t)\varepsilon_{20}(t)\alpha_{12} A_2 \tag{29}$$

and

$$i\dot{A}_2 - \left[\Delta - \frac{1}{4}\{\alpha_2(\omega_1)\varepsilon_{10}^2(t) + \alpha_2(\omega_2)\varepsilon_{20}^2(t)\}\right]A_2$$

$$= -\frac{1}{4}\varepsilon_{10}(t)\varepsilon_{20}(t)\alpha_{21} A_1,$$

where, as previously, Δ is the weak-field two-photon-resonance detuning (7).

Though not as nice as Eq. (11), Eqs. (29) are more convenient to describe the scaling effect existing in the system under consideration. Let us assume that both pulse envelopes $\varepsilon_{10}(t)$ and $\varepsilon_{20}(t)$ depend on time t only via the ratio t/τ, where τ is the pulse duration common for both high- and low-frequency pulses. Then, evidently, the arguments of the functions $\varepsilon_{10}(t)$ and $\varepsilon_{20}(t)$ do not change if we divide both t and τ by the same factor λ, $t \to t/\lambda$, and $\tau \to \tau/\lambda$. Moreover, one can see easily that Eqs. (29) do not change too if we multiply simultaneously both low- and high-frequency pulse peak intensities $I_{1,2} = c\varepsilon_{1,20}^2/8\pi$ and the weak-field detuning Δ by the same factor λ. So, the solutions of Eqs. (29) are

invariant with respect to the scaling transformation

$$\Delta \to \lambda\Delta, \quad \varepsilon_{1,20}^2 \to \lambda\varepsilon_{1,20}^2, \quad \tau \to \tau/\lambda, \quad t \to t/\lambda \quad (30)$$

with an arbitrary λ. This scaling effect can be important for practice: parameters of an assumed experiment can be varied to choose the most convenient conditions for observation the two-color stabilization effect discussed in this paper. In particular, by making laser pulses longer, one can use rather moderate-intensity lasers, as is shown below.

Owing to the the described scaling effect, it is convenient to introduce and use the dimensionless ratio of intensities x, interaction time θ and detuning δ,

$$x = \frac{I_2}{I_1}, \quad \theta = \tau I_1, \quad \delta = \frac{\Delta}{I_1}, \quad (31)$$

dimensionless complex quasienergies

$$y_\pm = \frac{\gamma_\pm - E_1 - \omega_1}{I_1}, \quad (32)$$

detuning for the ac Srark shifted and broadened levels (12)

$$\tilde{\delta} = \frac{\tilde{\Delta}}{I_1} = \delta - \frac{1}{4}\{\alpha_2(\omega_1) + \alpha_1(\omega_1) + [\alpha_1(\omega_2) + \alpha_2(\omega_2)]x\}, \quad (33)$$

and widths of the fully dressed quasienergy levels

$$g_\pm = \frac{\Gamma_\pm}{I_1} = -2\,\mathrm{Im}[y_\pm]$$

$$= \frac{1}{2}[\alpha_1''(\omega_1) + \alpha_1''(\omega_2)x] - \tilde{\delta}'' \mp \mathrm{Im}\left(\sqrt{\tilde{\delta}^2 + \frac{1}{4}\alpha_{12}^2 x}\right), \quad (34)$$

where $I_{1,2}$, Δ, τ, $\gamma_\pm$, and $\Gamma_\pm$ are in atomic units. Defined in such a way, quasienergies $y_\pm$ and widths $g_\pm$ depend only on two parameters x and δ, whereas the probability of ionization w_i and the residual probability to find an atom in bound states w_{res} (24)–(27) depend on three parameters x, δ, and θ.

VI. PULSE SHAPE

The concepts of quasienergies and quasienergy functions are very fruitful for an analysis exploiting a model of a rectangular pulse envelope. Such an analysis is useful for clarification of physics of the phenomenon under consideration. However, more realistic laser pulse shapes are characterized by smooth envelopes. To investigate a sensitivity of the results to be derived on the pulse shape and its smoothing, we will consider pulse envelopes $\varepsilon_{1,2}(t)$ of the form

$$\varepsilon_{1,20}(t) = \varepsilon_{1,20}\frac{(1+a)\sin^2\left[\pi\left(N(a)\frac{t}{\tau} + \frac{1}{2}\right)\right]}{1 + a\sin^2\left[\pi\left(N(a)\frac{t}{\tau} + \frac{1}{2}\right)\right]}, \quad (35)$$

where $\varepsilon_{1,20}=$const, $-1/2N(a) \leqslant t/\tau \leqslant 1/2N(a)$, $N(a)$ is the normalization factor
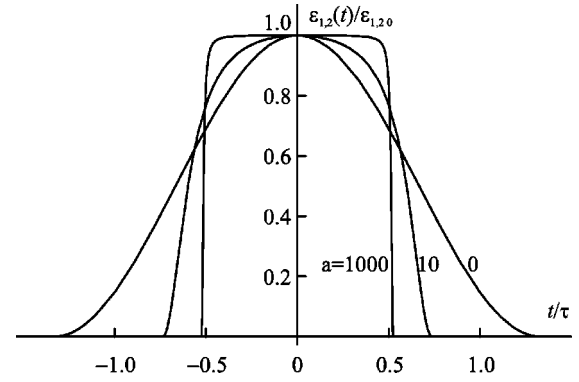

FIG. 4. Pulse envelopes (35) at three different values of the smoothing factor a.

$$N(a) = \frac{(1+a)^2}{a^2}\left\{1 - \frac{2+3a}{2(1+a)^{3/2}}\right\} \quad (36)$$

such that

$$\int_{-\tau/2N}^{\tau/2N} \varepsilon_{1,20}^2(t)dt = \tau\,\varepsilon_{1,20}^2, \quad (37)$$

and a is a smoothing parameter. At $a \to \infty$, $N(a) \to 1$ and the envelopes $\varepsilon_{1,20}(t)$ (35) turn into the rectangular ones. At $a = 0$, $N(0) = 3/8$, and $\varepsilon_{1,20}(t)$ (35) takes the form of a pure $\sin^2$ pulse envelope

$$\varepsilon_{1,20}(t) = \varepsilon_{1,20}\sin^2\left[\pi\left(\frac{3t}{8\tau} + \frac{1}{2}\right)\right]. \quad (38)$$

By definition, for the pulse envelopes of the form (35), at all values of the smoothing factor a the peak values of the field strengths and areas under the curves $\varepsilon_{1,2}^2(t)$ (field energy per unit cross section) are kept constant and equal to $\varepsilon_{1,20}$ and $\varepsilon_{1,20}^2\tau$, correspondingly (see Fig. 4). Hence, at all a the parameter τ can be interpreted as the pulse duration determined by the condition (37). For all a the dimensionless pulse duration is determined as previously, $\theta = I_1 \times \tau$ with both I_1 and τ taken in atomic units.

VII. OPTIMIZATION OF THE LEVEL-NARROWING EFFECT

Optimization of the stabilization and level-narrowing effects assumes minimization of the width of the narrower quasienergy level $g_+(\delta,x)$ with respect to two variables δ and x. As a first step in a solution of this problem, let us minimize $g_+(\delta,x)$ with respect to the field-free detuning δ at a given x. Typically, at any given x, in dependence on δ, the functions $g_\pm(\delta,x=\text{const})$ have well pronounced minimum and maximum (Fig. 5).

Specifically, the curves of Fig. 5 are calculated for a He atom at $x=0.1$. Details of these and many other calculations, as well as the data about frequencies, atomic levels, and polarizability tensors are given in the following section. Here the picture of Fig. 5 is shown as a typical example of the dependencies $g_\pm(\delta,x=\text{const})$. To find a position of the extre-
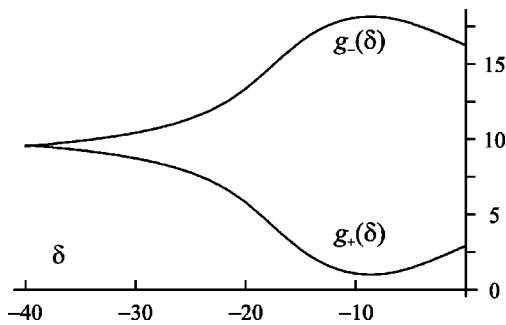
FIG. 5. The functions $g_\pm(\delta) \equiv g_\pm(\delta, x = \text{const})$ (33).

mum shown in Fig. 5, $\delta_{\text{opt}}(x)$, we have to solve the equation $dg_\pm(\delta)/d\delta = 0$. Direct calculations show that this condition is satisfied if $\text{Im}\{[\widetilde{\delta}\alpha_{12}^*]^2\} = 0$, which gives two equations $\text{Re}[\widetilde{\delta}\alpha_{12}^*] = 0$ and $\text{Im}[\widetilde{\delta}\alpha_{12}^*] = 0$. It can be checked directly that only the second of these two equations corresponds to the extremum we are looking for, and this equation gives

$$\alpha_{12}'\,\widetilde{\delta}'' - \alpha_{12}''\,\widetilde{\delta}' = 0, \quad \widetilde{\delta}_{\text{opt}} = \frac{\alpha_{12}}{\alpha_{12}''}\widetilde{\delta}', \tag{39}$$

or

$$\delta_{\text{opt}}(x) = \frac{1}{4}\left\{\alpha_2'(\omega_1) - \alpha_1'(\omega_1) - \frac{\alpha_{12}'}{\alpha_{12}''}[\alpha_2''(\omega_1) - \alpha_1''(\omega_1)]\right\} + \frac{x}{4}\left\{\alpha_2'(\omega_2) - \alpha_1'(\omega_2) - \frac{\alpha_{12}'}{\alpha_{12}''}[\alpha_2''(\omega_2) - \alpha_1''(\omega_2)]\right\}. \tag{40}$$

As explained above, $\delta_{\text{opt}}(x)$ is a value of the field-free detuning, at which the width of one of the two quasienergy levels (γ_+) has a minimum with respect to δ at arbitrary given x. As is seen from Eq. (40) the optimal detuning $\delta_{\text{opt}}(x)$ is a linear function of the ratio of intensities $x = I_2/I_1$. Note that the linear dependence of δ_{opt} on I_2 at a given I_1 agrees with one of the results of Ref. [9].

The second step in optimization conditions for stabilization requires minimization of the width g_+ calculated at $\delta = \delta_{\text{opt}}(x)$ with respect to the variable x. With the help of the second equation (39) the "δ-optimized" widths $g_\pm(\delta_{\text{opt}}(x), x)$ can be reduced to the following rather simple form:

$$g_\pm(\delta_{\text{opt}}(x), x) = \frac{1}{2}\alpha_1''(\omega_1) - \widetilde{\delta}_{\text{opt}}''(x) \mp \sqrt{[\widetilde{\delta}_{\text{opt}}''(x)]^2 + \frac{1}{4}\alpha_{12}''^2 x}, \tag{41}$$

where

$$\widetilde{\delta}_{\text{opt}}''(x) = -\frac{1}{4}[\alpha_2''(\omega_1) - \alpha_1''(\omega_1) + \alpha_2''(\omega_2)x], \tag{42}$$

and in Eqs. (41) and (42) we have put $\alpha_1''(\omega_2) = 0$, which is true in the case $\omega_2 < |E_1|$.

By using Eqs. (41) and (42) we can find easily the asymptotic expansion of the function $g_+(\delta_{\text{opt}}(x), x)$ in powers

of $1/x$ at large x, $x \gg 1$. The constant term in this expansion vanishes and the first nonzero term is given by

$$g_+(\delta_{\text{opt}}(x), x) \approx \frac{1}{2x}\frac{\alpha_1''(\omega_1)\alpha_2''(\omega_1)}{\alpha_2''(\omega_2)}. \tag{43}$$

This result shows that at large x the width of the narrower quasienergy level g_+ decreases and tends zero as $1/x$. This is an indication of a possibility of the unlimited narrowing of this quasienergy level and, hence, achievement of a very high degree of stabilization. Real limitations of narrowing and stabilization are determined by the applicability conditions of the model. For example, at very large values of x the second-field intensity can become too high for the ATI processes in this field to be ignored. In accordance with Eq. (40), at the optimal conditions the increase of x is accompanied by a linear increase of the field-free detuning δ. This gives other limitations for the growth of x: at sufficiently large detunings the influence of atomic levels different from E_1 and E_2 and not taken into account in the model can become important. At last at very large δ even the above rotating wave approximation can become invalid. But, on the other hand, these limitations are not too severe, and rather significant level of narrowing and stabilization of an atom can be reached under quite realistic conditions. These conclusions, as well as the general result about asymptotic decrease of the narrower-level width at large x are confirmed and specified in the following section by direct numerical calculations for hydrogen and helium atoms.

It should be noted that the curve $\delta_{\text{opt}}(x)$ includes the point (δ_0, x_0) where the complex detuning between the ac-Stark shifted and broadened levels (15) turns zero, $\widetilde{\delta} = 0$. At this point

$$x_0 = \frac{\alpha_1''(\omega_1) - \alpha_2''(\omega_1)}{\alpha_2''(\omega_2) - \alpha_1''(\omega_2)} \tag{44}$$

and, in accordance with Eq. (40),

$$\delta_0 = \frac{1}{4}\{\alpha_2'(\omega_1) - \alpha_1'(\omega_1) + x_0[\alpha_2'(\omega_2) - \alpha_1'(\omega_2)]\}. \tag{45}$$

VIII. NUMERICAL CALCULATIONS FOR A He ATOM

All the required numerical data are known for selected levels in hydrogen and helium atoms. To a very large extent, the results obtained for these two atoms appear to be very similar. For this reason, below, the results of calculation of a helium atom are described in detail, and then a short sketch of calculations for a hydrogen atom is given to demonstrate mainly the arising differences and peculiarities of each atom.

A. Widths of quasienergy levels

Let us consider the following two levels of a He atom and the following two frequencies: $1s2s \equiv E_1$ and $1s4s \equiv E_2$ and $\omega_1 = 8.44$ eV (the second harmonic of a dye laser) and $\omega_2 = 1,17$ eV (Nd:YAG laser). For these levels and frequencies
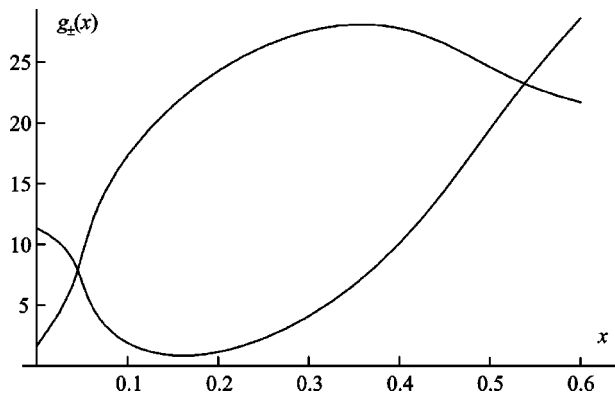
FIG. 6. The relative widths of quasienergy levels of a He atom $g_\pm(x)$ calculated at $\delta = \delta_0$ (47).

FIG. 7. Three typical curves $g_+(\delta = \text{const}, x)$ for He calculated at $\delta = -11$, -15, and -23 (from the left to the right)

all the polarizability tensor components (8), (9) are known [23,24], and in atomic units they are equal to

$$\alpha_1(\omega_1) = -30.42 + i\,22.65, \quad \alpha_1(\omega_2) = -236.6,$$

$$\alpha_2(\omega_1) = -45.66 + i\,3.21, \quad \alpha_2(\omega_2) = -479.96 + i\,124.55,$$

$$\alpha_{12} = 38.74 + i\,53.07. \tag{46}$$

The point where the dressed-level detuning $\widetilde{\Delta}$ (15) [or $\widetilde{\delta}$ (33)] turns zero, $\widetilde{\Delta} = \widetilde{\delta} = 0$, has the following coordinates in the plane $\{x, \delta\}$:

$$x_0 = 0.156 \quad \text{and} \quad \delta_0 = -13.3. \tag{47}$$

The relative width of the fully dressed quasienergy levels $g_\pm$ (34) are shown in Fig. 6 in their dependence on x at $\delta = \delta_0$. At this value of the detuning δ, the curves $g_+(x)$ and $g_-(x)$ cross each other twice. The left and right crossings turn into the avoided crossings, correspondingly, at $\delta \gtrsim -11.3$ and $\delta \lesssim -22.4$, and both crossings never turn into avoided crossings together.

For the polarizability tensor of Eq. (46), the expression (40) for the optimal-narrowing detuning $\delta_{\text{opt}}(x)$ takes the form

$$\delta_{\text{opt}}(x) = -0.26 - 83.57\,x. \tag{48}$$

In the picture of Fig. 7 the width $g_+(\delta, x)$ of the narrower quasienergy level is plotted in its dependence on the intensity ratio x at three different given values of the field-free detuning δ. The curve at $\delta = -11$ differs qualitatively from two other curves. The difference arises because for this curve the detuning δ is large enough for the left crossing of Fig. 6 to turn into the avoided crossing. The sharp peak of the curve $g_+(\delta = -11, x)$ at Fig. 7 is an indication of the root-square branch-point-like behavior, which takes place at $\delta = -11.3$ and which is similar to the root-square branch-point behavior of the curve of Fig. 1 for $\gamma''_\pm$ in an idealized two-level system of Sec. I A.

The minima of all three curves at Fig. 7 are seen to be getting deeper the larger is $|\delta|$. Positions of these minima $x^{\min}(\delta)$ are determined by the optimal detuning (48) and can
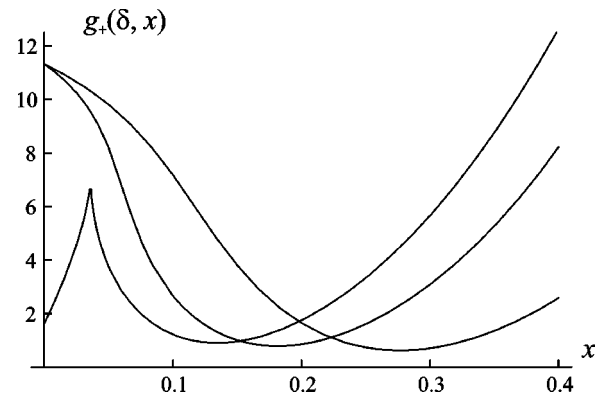
be found from the equation $\delta = \delta_{\text{opt}}(x)$. The x-dependent width of the narrower quasienergy level, minimized with respect to δ, is given by $g_+^{\min}(x) \equiv g_+(\delta_{\text{opt}}(x), x)$, and its dependence on x is given by the curve of Fig. 8.

A monotonous fall of the function $g_+^{\min}(x)$ means that the x-dependent width of the narrower quasienergy level, minimized with respect to the detuning δ, tends to zero at asymptotically large values of x. In other words, in the framework of the used model one of the two quasienergy levels of the system can be narrowed unlimitedly by means of increasing the ratio of intensities $x = I_2/I_1$ and the field-free detuning $|\delta|$ in such a way that the equation $\delta = \delta_{\text{opt}}(x)$ remains satisfied. Real limitations of such a narrowing are determined only by the model applicability conditions: (i) at very large values of x the second-field intensity I_2 will become too high to ignore above-threshold ionization produced by this field and (ii) at very large values of $|\delta|$ other levels ignored above can become more important and, at $|\Delta| \sim \omega_2$, the rotating-wave approximation can become invalid. But at sufficiently long pulse durations τ and low first-field intensity I_1 these limitations are not too severe, and the achievable degree of narrowing can be rather high.

B. Probabilities of ionization and nonionization

The residual probabilities to find a He atom in its bound states after interaction with a two-color field in the case of a
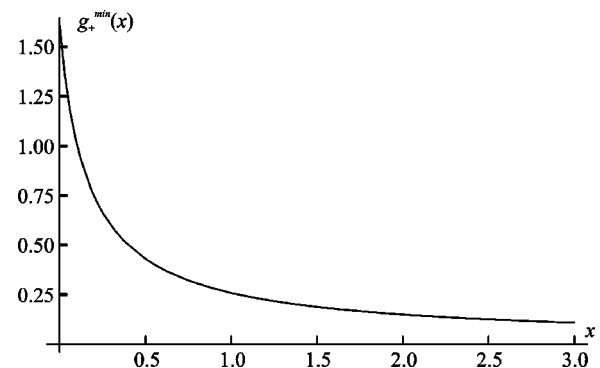

FIG. 8. The width of the narrower quasienergy level of a helium atom $g_+^{\min}(x)$, minimized with respect to the detuning δ, in its dependence on x.
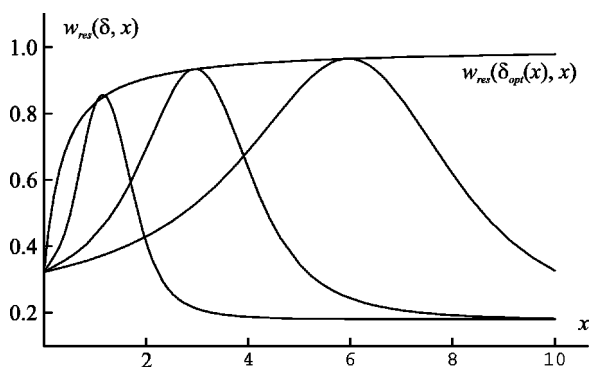
FIG. 9. The residual probability to find a He atom in bound states calculated at $\delta = -100$, -250, and -500 (from the left to the right) and $\delta = \delta_{\mathrm{opt}}(x)$ (48) (the upper curve), $\theta = 0.1$.

rectangular envelope is determined by Eqs. (24), (26), and (27), and the results of the corresponding calculations are shown in Fig. 9. The three resonance like curves correspond to three different values of the field-free detuning δ. The envelope of peaks of these curves is the maximized residual probability equal to $w_{\mathrm{res}}(\delta_{\mathrm{opt}}(x), x)$ with $\delta_{\mathrm{opt}}(x)$ given by Eq. (48). These results show that the function $w_{\mathrm{res}}(\delta_{\mathrm{opt}}(x), x)$ monotonously grows approaching one at large values of x. This means that under optimal conditions stabilization of a He atom in a two-color field can be very high, more than 90%.

The picture of Fig. 10 shows the distribution of the residual probability between the levels E_1 and E_2. Under the conditions of optimal stabilization [$\delta = \delta_{\mathrm{opt}}(x)$] at sufficiently high value of the intensity ratio x, the ratio of probabilities w_1/w_2 falls tending asymptotically to zero. This means that under the optimal stabilization conditions, interference suppresses not only ionization but also excitation of the level E_2, which can be seen experimentally also.

In all pictures of this section (Figs. 6–10) the calculated values are plotted in their dependence on the intensity ratio x. To see such dependencies in experiments one has to make, for example, a series of measurements at different values of the second-field intensity I_2 at a given first-field intensity I_1. Another possible way of an experimental investigation is keeping the ratio $x = I_2/I_1$ constant and changing both intensities synchronously. Calculated for such a scheme of mea-
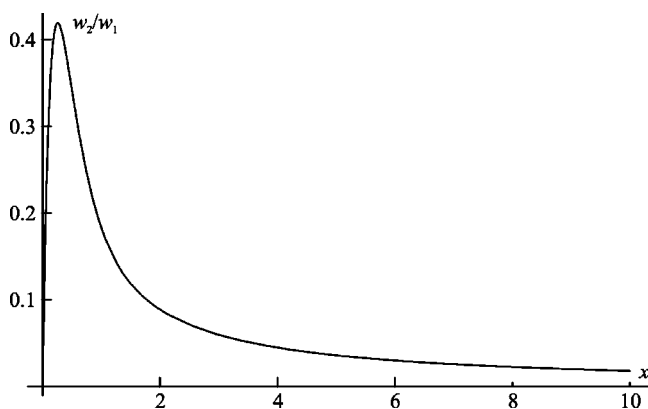

FIG. 10. The ratio w_2/w_1 for a He atom at $\delta = \delta_{\mathrm{opt}}(x)$ (48), $\theta = 0.1$.
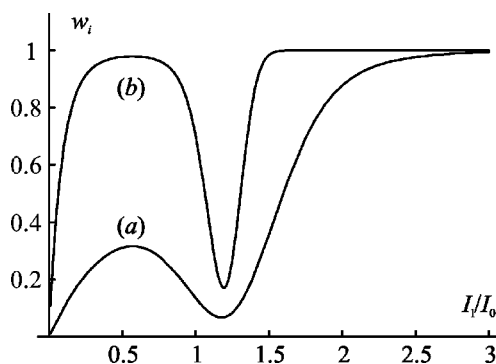

FIG. 11. $w_i(I_1/I_0)$ at $I_2 = 3I_1$, $\delta = -300(I_0/I_1)$ and $\theta = 0.1(I_1/I_0)$ (a) and I_1/I_0 (b).

surements, the probability of ionization in its dependence on $I_1 \propto I_2$ is given by the curves of Fig. 11. In this picture the intensity I_1 is expressed in units of an arbitrary constant intensity I_0 at $x = I_2/I_1 = 3$. The detuning Δ and pulse duration τ are taken to be equal to $\Delta = -200I_0$ and $\tau = 0.1/I_0(a)$ or $\tau = 1/I_0(b)$, where Δ, τ, and I_0 are in atomic units.

Normalization by an arbitrary constant I_0 reflects the scaling effect described above in Sec. V. A possibility to choose any value of I_0 indicates a large flexibility of the system under consideration with respect to a choice of of the light intensities and pulse durations. For example, if $I_0 = 10^{-6}$ a.u. ($\approx 3 \times 10^{10}$ W/cm^2), the intensity $I_2 = 3 \times I_1$ does not exceed 3×10^{11} W/cm^2 in the variation range of I_1 at Fig. 11, which is low enough for no ATI effects to take place. And, under the best stabilization conditions, the detuning Δ and pulse duration are equal to $\Delta = -240I_0 = -2.4 \times 10^{-4}$ a.u. ~ 0.065 eV $\ll \omega_{1,2}$ and $\tau = 1/I_0 = 10^6$ a.u. ~ 3 ps.

The curves of Fig. 11 are typical for the stabilization picture. With a growing light intensity, at first, the probability of ionization grows (perturbation theory region), then falls, and this is the beginning of the stabilization window, and finally grows again, which corresponds to the break of stabilization. Stabilization and its break arise because, owing to the ac Stark shift and level mixing, with a growing light intensity the system comes to and, then, goes out of the resonance conditions, optimal for fully dressed-level narrowing and interference stabilization. Curve (b) of Fig. 11 indicates an appearance of an additional region between the perturbation theory and stabilization zone at a sufficiently long pulse duration τ. This is the region of the total ionization of an atom, where $w_i = 1$. This means that at some intermediate intensity light pulses provide a complete ionization and at a stronger field, owing to interference, ionization becomes rather small ($w_i \sim 0.2$). In absolute values, the minimal achievable probability in the stabilization region is somewhat lower in the case of short pulses ($\tau = 0.1 I_1/I_0$) [curve (a) of Fig. 11]. But the degree of stabilization can be determined alternatively as the ratio of the maximal probability achievable in the region between perturbation theory and stabilization regions to the minimal value of w_i in the stabilization window. In terms of such a definition, the degree of stabilization is much higher in the case of longer pulses ($\tau = I_1/I_0$) [curve (b) of Fig. 11]. Of course, a further increase of the pulse duration flattens the curve of Fig. 11 in the stabilization region and decreases the
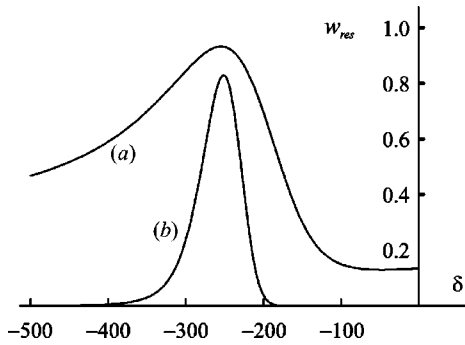
FIG. 12. $w_{\text{res}}(\delta)$ at $I_2 = 3I_1$, $I_1 = 1.2I_0$, $\theta = 0.12$ (a), and 1.2 (b).

degree of stabilization. In this sense, the pulse duration chosen for the curve b of Fig. 11, $\tau = I_1/I_0$, is close to the optimal one.

The picture of Fig. 12 characterizes spectral features of the residual probability to find an atom in its bound states at the best stabilization conditions of Fig. 11: $I_2/I_1 = 3$, $I_1/I_0 = 1.2$, $\theta = 0.12$ (a) and 1.2 (b) (which corresponds to $\tau = 0.1/I_0$ and $\tau = 1/I_0$).

Curve (a) of this picture looks similar to the Fano curve of Fig. 1. This shows that at $\tau = 0.12/I_0$, still, the effect of stabilization under discussion can be interpreted as a strong-field LICS. But in the case of longer pulses, $\tau = 1.2/I_0$ [curve (b) of Fig. 12] similarity with LICS practically disappears. The only reminder about a remote connection with the Fano curve is a slight asymmetry of the curve b of Fig. 12. Apart from this, curve (b) describes the effect of interference stabilization in its pure form.

C. Smooth envelope

All the results described above were derived for pulses with a rectangular envelope. Usually, envelopes of short laser pulses are smooth. To consider such a more realistic situation, we have solved general equations (11) with the $\sin^2$ pulse envelopes (38). The results of such a solution are shown in Fig. 13, which is a direct analog of Fig. 9. Again, a series of resonancelike curves describes the residual probability of finding an atom in its bound states $w_{\text{res}}(\delta, x)$ at various given values of the detuning δ and the intensity ratio x considered as the independent variable. The residual probability maximized with respect to the detuning δ is the envelope of the peaks of these curves. In Fig. 13 such a maximized probability is approximated by the functions $w_{\text{res}}(\delta_{\text{opt}}^{\sin}(x), x)$, where $\delta_{\text{opt}}^{\sin}(x)$ is the empirically found linear function providing the best fitting to the peak envelope.

$$\delta_{\text{opt}}^{\sin}(x) = 3.122 - 73.3\, x. \qquad (49)$$

In Fig. 14 we plot the maximized residual probability to find He atoms in bound states calculated in the cases of rectangular (curves 1 and 2) and $\sin^2$ (curve 3) pulse envelopes at $\delta = \delta_{\text{opt}}^{\text{rect}}(x)$ (48) (the curve 1) and $\delta = \delta_{\text{opt}}^{\sin}(x)$ (49) (curves 2 and 3). Comparison of curves 1 and 3 shows that a transition to a smooth envelope $\varepsilon_0(t)$ reduces a little bit the maximal achievable degree of stabilization compared to the rectangular-envelope case, but not too much (70–75 % in-
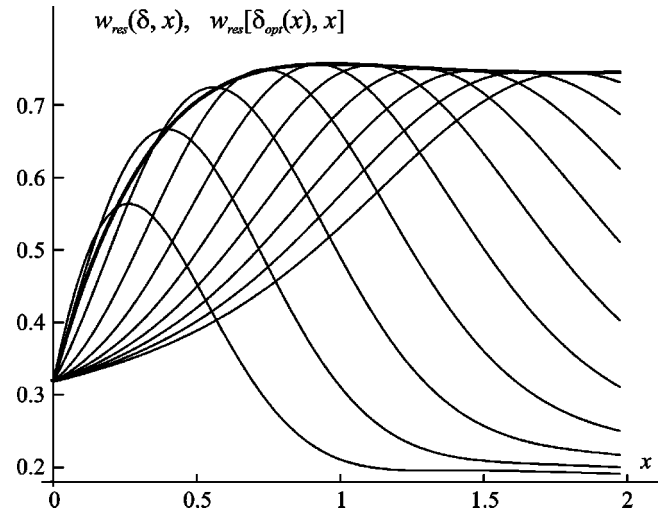

FIG. 13. A series of curves $w_{\text{res}}(\delta, x)$ at various given values of the detuning δ and the function $w_{\text{res}}[\delta_{\text{opt}}^{\sin}(x), x]$ (a thick curve) for a He atom and the $\sin^2$ pulse envelopes [Eq. (38)].

stead of 90%). Moreover, curve 3 of Fig. 14 shows that in the case of a smooth pulse envelope the residual probability remains more or less stable in a rather large variation interval of the intensity ratio x, approximately from 0.5 to 5 and more. This shows that the effect of stabilization is rather robust.

Another interesting effect seen rather well from comparison of curves 2 and 3 of Fig. 14. These two curves are calculated at the coinciding dependencies of the detuning δ on the intensity ratio parameter x, $\delta = \delta_{\text{opt}}^{\sin}(x)$ (49). As is seen well from Fig. 14, at $x \lesssim 1$ the curve 3 goes above the curve 2. This means that at the same detunings the residual probability to find an atom in its bound states in the case of smooth envelope pulses exceeds the same probability at a rectangular pulse envelope. In other words, in this range of the intensity ratio parameter x smoothing of the pulse envelope increases rather than reduces the degree of stabilization. This conclusion follows directly from calculations though it looks counterintuitive and, in this sense, rather interesting.
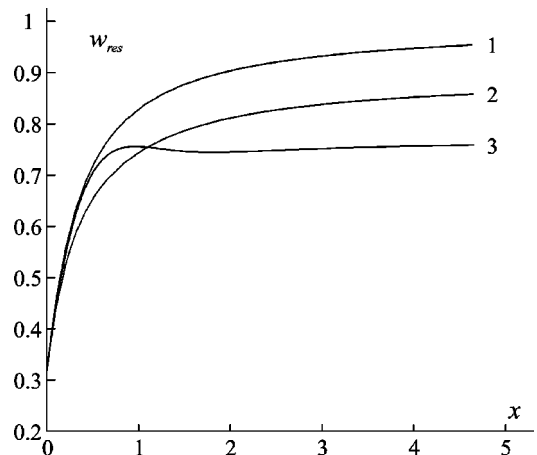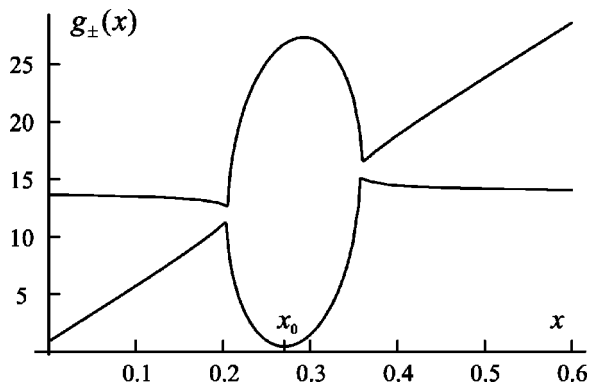

FIG. 14. The functions $w_{\text{res}}^{\text{rect}}[\delta_{\text{opt}}^{\text{rect}}(x), x]$ (1), $w_{\text{res}}^{\text{rect}}[\delta_{\text{opt}}^{\sin}(x), x]$ (2), and $w_{\text{res}}^{\sin}[\delta_{\text{opt}}^{\sin}(x), x]$ (3) with $\delta_{\text{opt}}^{\text{rect}}(x)$ and $\delta_{\text{opt}}^{\sin}(x), x$ given by Eqs. (48) and (49), respectively.

FIG. 15. The functions $g_\pm(\delta_0,x)$ (33).

IX. HYDROGEN

In a hydrogen atom, all the polarizability tensor components are known for the levels $2s$ and $5s$ and frequencies $\omega_1=4.02$ eV (XeCl laser) and $\omega_2=1.17$ eV (Nd:YAG laser) [10]. In atomic units they are given by

$$\alpha_1(\omega_1) = -45.56 + i\,27.29, \quad \alpha_1(\omega_2) = 179.92,$$

$$\alpha_2(\omega_1) = -45.66 + i\,1.78, \quad \alpha_2(\omega_2) = -513.76 + i\,93.83,$$

$$\alpha_{12} = 6.56 + i\,50.60. \qquad (50)$$

The data (50) show, in particular, that $\Gamma_2^{(1)}/\Gamma_1 = \alpha_2''(\omega_1)/\alpha_1''(\omega_1) \sim 6.5 \times 10^{-2}$, which means that the assumption (18) is pretty well satisfied.

Rigorously, in a hydrogen, there are other levels ($5d$ and $5f$) of almost the same energy as $5s$. Owing to the selection rules, the level $5f$ is not connected either with $2s$ or $5s$ levels by two-photon Raman-type transitions and, for this reason, can be ignored. As for the level $5d$, in principle, it can participate in a scheme of two-photon Raman-type transitions under consideration. However, by ignoring at first this additional level let us consider a two-level $2s$-$5s$ scheme, analogous to that of the previous section.

For this system the coordinates of the $\tilde{\delta}=0$ point in the $\{x, \delta\}$ plane are given by

$$x_0 = 0.272, \quad \delta_0 = -47.2. \qquad (51)$$

At $\delta = \delta_0$, the calculated relative width of the fully dressed quasienergy levels $g_\pm$ (34) in their dependence on x are shown in Fig. 15.

Compared with Fig. 5, the picture of Fig. 15 indicates the first well pronounced difference between helium and hydrogen. In the case of hydrogen the curves of widths of quasienergy levels vs x have two avoided-crossing points whereas in the case of helium such a situation never occurs and at $\delta = \delta_0$ there are two real-crossing points (Fig. 5).

Another important difference concerns smooth pulse envelopes and the third level effect. To solve such a problem, we have to generalize Eqs. (10) and (11). In Eq. (10), in accordance with the more general Eq. (4), there appears an additional term $C_3(t)e^{i\omega_2 t}\psi_3$. Then, equations for $C_i(t)(i=1,2,3)$ take the form
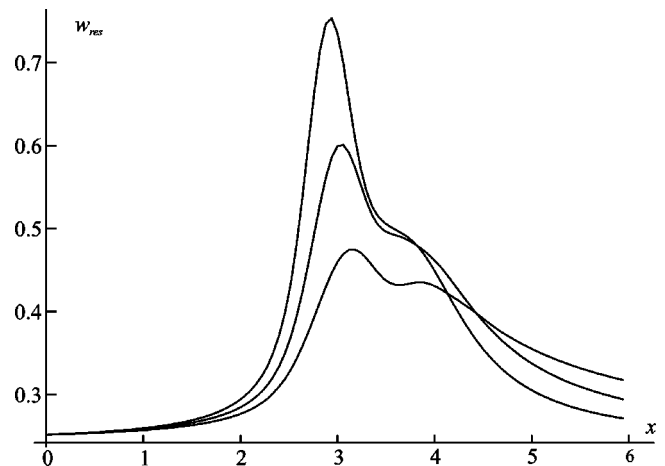
FIG. 16. The function $w_{\text{res}}(x)$ in a three-level scheme at $\delta = -530$, $\theta=0.1$, and the envelope smoothing parameter in Eq. (35) $a=100, 10$, and 0.1 (from top to bottom).

$$i\dot{C}_1 - [\widetilde{E}_1(t) + \omega_1]C_1 = -\frac{1}{4}\varepsilon_{10}(t)\varepsilon_{20}(t)(\alpha_{12}C_2 + \alpha_{13}C_3),$$

$$i\dot{C}_2 - [\widetilde{E}_2(t) + \omega_2]\,C_2 = -\frac{1}{4}\varepsilon_{10}(t)\varepsilon_{20}(t)\alpha_{21}C_1$$

$$-\frac{1}{4}[\alpha_{23}(\omega_1)\varepsilon_{10}^2(t)$$

$$+ \alpha_{23}(\omega_2)\varepsilon_{20}^2(t)]\,C_3(t),$$

$$i\dot{C}_3 - [\widetilde{E}_3(t) + \omega_2]\,C_3 = -\frac{1}{4}\varepsilon_{10}(t)\varepsilon_{20}(t)\alpha_{13}C_1$$

$$-\frac{1}{4}[\alpha_{23}(\omega_1)\varepsilon_{10}^2(t)$$

$$+ \alpha_{23}(\omega_2)\varepsilon_{20}^2(t)]\,C_2(t) \qquad (52)$$

where $\widetilde{E}_3$ is given by the same Eq. (12) as $\widetilde{E}_1$ and $\widetilde{E}_2$ with $\alpha_3(\omega_{1,2})$ and new off-diagonal elements of the polarizability tensor given by [10]

$$\alpha_3(\omega_1) = -43.26 + i\,0.42, \quad \alpha_3(\omega_2) = -405.9 + i\,81.8,$$

$$\alpha_{23}(\omega_1) = 0.74 + i\,0.21, \quad \alpha_{23}(w_2) = 68.61 + i\,21.63,$$

$$\alpha_{13} = 6.15 + i\,11.69. \qquad (53)$$

Found from Eqs. (52) and (35) the residual probability to find an atom in its bound states is shown in Fig. 16 for three different values of the pulse envelope smoothing factor a.

Two rather interesting conclusions can be deduced from this picture. First, a strong smoothing of pulse envelopes decreases the peak value of the residual probability to find an atom in bound states. At the chosen value of the detuning $\delta = -530$ in the case of pure $\sin^2$ pulses $[w_{\text{res}}(x)]_{\max}$ is almost twice as small as in the case of rectangular envelopes. The

smoothing induced decrease of the residual probability in the case of hydrogen is much more significant than in the case of helium.

The second effect seen in the picture of Fig. 16 concerns the influence of the third level. This influence manifests itself in a shoulder on the curves $w_{\mathrm{res}}(x)$, but the third level is seen not to affect the main maximum of the curves much.

X. CONCLUSION

To summarize, we describe and discuss a scheme of interaction of atoms with radiation of two lasers. Intensity and pulse duration of lasers are assumed to be high and long enough to provide full ionization in the field of each of these two lasers alone if only atoms are prepared initially at levels from which one-photon ionization can take place. We show that owing to interference effects under the conditions close to Raman-type resonance between some two selected atomic levels ionization of an atom experiencing a joint action of the field of two lasers can be significantly (up to 90%) suppressed. Optimization of such a stabilization effect involves optimization with respect to the Raman-type resonance de-

tuning and the ratio of the two laser intensities. Specific calculations are carried out for hydrogen and helium atoms for couples of atomic levels and laser frequencies at which information about the complex polarizability tensors involved is available. Qualitatively, the results of calculations for hydrogen and helium appear to be very similar. This gives us a reason to think that the effect described is rather universal, and can occur also at other atoms, levels, and frequencies. The dependence of the effect on laser pulse shapes is investigated. It is shown that in the case of helium atoms sensitivity of the results to a pulse shape is lower than in the case of hydrogen atoms. In helium, even in the case of smooth pulses, the degree of stabilization remains rather high (more than 70%), and the effect exists at this level in a rather large range of the intensity ratio parameter x. The described scaling effect gives a possibility to select ranges of variation of the laser pulse peak intensities and pulse duration in ranges most convenient for experimental observation.

[1] M. V. Fedorov and A. M. Movsesian, J. Phys. B **21**, L155 (1988).

[2] M. V. Fedorov, *Atomic and Free Electrons in a Strong Light Field* (World Scientific, Singapore, 1997).

[3] L. Armstrong, Jr., B. Beers, and S. Feneuille, Phys. Rev. A **12**, 1903 (1975).

[4] Yu. I. Heller and A. K. Popov, Opt. Commun. **18**, 449 (1976).

[5] A. I. Andryushin and M. V. Fedorov, Izv. Vuzov: Fiz. **1**, 63 (1978) [Sov. Phys. J. **1**, 49 (1978)].

[6] Bo-nian Dai and P. Lambropulos, Phys. Rev. A **36**, 5205 (1987).

[7] M. V. Fedorov and A. E. Kazakov, Prog. Quantum Electron. **13**, 97 (1989).

[8] P. L. Knight *et al.*, Phys. Rep. **190**, 1 (1990).

[9] N. J. Kylstra *et al.*, J. Phys. B **31**, L719 (1998).

[10] A. I. Magunov, I. Rotter, and S. I. Strakhova, J. Phys. B **34**, 29 (2001).

[11] M. H. R. Hutchinson and K. M. M. Ness, Phys. Rev. Lett. **60**, 105 (1988).

[12] Y. L. Shao *et al.*, Phys. Rev. Lett. **67**, 3669 (1991).

[13] S. Cavalieri and F. S. Pavone, Phys. Rev. Lett. **67**, 3673 (1991).

[14] T. Halfmann *et al.*, Phys. Rev. A **58**, 46 (1998).

[15] K. Rzazewski and J. H. Eberly, Phys. Rev. Lett. **47**, 408 (1981).

[16] P. Lambropoulos and P. Zoller, Phys. Rev. A **24**, 379 (1981).

[17] A. I. Andryushin, M. V. Fedorov, and A. E. Kazakov, J. Phys. B **15**, 2851 (1982).

[18] A. Lami and N. K. Rahman, Phys. Rev. A **26**, 3360 (1982); **33**, 782 (1986); **34**, 3908 (1986); **40**, 2385 (1989).

[19] G. Alzetta, A. Gozzinin, L. Moi, and G. Orriols, Nuovo Cimento Soc. Ital. Fis., B **36**, 5 (1976).

[20] E. Arimondo and G. Orriols, Lett. Nuovo Cimento Soc. Ital. Fis. **17**, 333 (1976).

[21] R. M. Whitley and C. R. Stroud, Phys. Rev. A **14**, 1498 (1976).

[22] E. Arimondo, Prog. Opt. **35**, 257 (1996).

[23] L. P. Yatsenko, T. Halfman, B. W. Shore, and K. Bergmann, Phys. Rev. A **59**, 2926 (1999).

[24] A. I. Magunov and S. I. Strakhova, Quantum Electron. **33**, 231 (2003).